ЖУРНАЛ ФІЗИЧНИХ ДОСЛІДЖЕНЬ
т. 2, № 3 (1998) с. 290–295

JOURNAL OF PHYSICAL STUDIES
v. 2, No. 3 (1998) p. 290–295

# PHENOMENOLOGICAL $S$–MATRIX APPROACH TO STUDY OF THE $^6$Li SCATTERING BY NUCLEI

V. V. Pilipenko
*Kharkiv State University, 4 Svobody Sq., Kharkiv, UA–310077, Ukraine*
(Received May 29, 1997; received in final form May 7, 1998)

The recently proposed original $S$–matrix model is employed for analyzing cross sections of the $^6$Li elastic scattering by different target nuclei at different energy values. The results of analysis are compared with those obtained by the optical model.

**Key words:** lithium 6 reactions, elastic scattering, differential cross sections, $S$–matrix, optical potential.

PACS number(s): 24.10.Ht, 25.70.–z

## I. INTRODUCTION

A study of the refraction effects in the differential cross sections of nuclear scattering at projectile energies $E$ >20–30 MeV/nucleon is of considerable interest for investigation of the interaction between colliding nuclei. Owing to the strong absorption of scattered waves, the cross section patterns at small scattering angles are of diffraction character. They are governed by the collision geometry, i.e. they are mainly determined by radii of the nuclei and surface diffuseness, as well as by the strength of the Coulomb interaction [1, 2]. For this reason, they are not very sensitive to details of the interaction, in particular, at short distances. However, at sufficiently high energies the scattering cross sections of light nuclei measured in a wide angular range manifest deviations from the diffraction behavior, which are caused by strong nuclear refraction (the nuclear rainbow effect and the Fraunhofer crossovers [2]). Analysis of the nuclear scattering cross sections in the region of the rainbow maxima and Fraunhofer crossovers shows that they are fairly sensitive to the choice of interaction model and allows one to probe the interaction region to short distances. The prevalent approach to analyzing elastic nuclear scattering in the intermediate energy region is the optical model which describes successfully both the diffraction scattering patterns and various refraction effects [2–4].

An alternative method of describing cross sections of the processes under consideration is the $S$–matrix approach which makes use of certain parametrizations of the scattering matrix [5–8]. Unfortunately, at present the $S$–matrix approach, being as valuable as the potential one and having certain advantages of its own, is much less developed, than the optical model. Simple forms of the $S$–matrix [5, 6] take account of the presence of a strong nuclear absorption, as well as of a weak nuclear refraction in the nuclear surface region. This model describes the cross sections of the diffraction type fairly well. Parametrization [7] which involves a nuclear rainbow point takes a more careful account of nuclear refraction and, in some cases, was able to describe refraction effects for the scattering of carbon and oxygen heavy ions [9]. However, the $S$–matrix models [5–7] cannot, as a rule, describe satisfactorily the pronounced refractive behavior of the cross sections which is observed for light ion scattering. Therefore, it is of interest to develop an $S$–matrix approach which would make it possible to analyze scattering of different ions in wide ranges of incident energies, scattering angles, and target mass numbers.

In [10, 11] an original $S$–matrix parametrization was proposed for analyzing the nuclear rainbow effect, which turned out to describe successfully various patterns of heavy ion scattering, as well [12, 13]. In particular, in [12] an analysis was carried out of cross sections of the 156 MeV $^6$Li elastic scattering by $^{12}$C, $^{40}$Ca, and $^{90}$Zr nuclei. In the present paper, the $S$–matrix approach proposed is used for further analysis of the refraction effects in the $^6$Li elastic scattering by various nuclei at different energy values (210 and 318 MeV), and the results obtained, together with those from the previous analysis at 156 MeV [12], are compared with the results of optical–model calculations.

## II. DESCRIPTION OF THE $S$–MATRIX MODEL

Since the $^6$Li elastic scattering cross sections in the energy region under consideration are not sensitive to the spin–orbit part of interaction, we neglect the spin dependence of the $S$–matrix. Then, the parametrization which we use to analyze the experimental data contains, like the standard optical model, six parameters. The $S$–matrix, as a function of the angular momentum $L = l + 1/2$, is represented in the form

$$S(L) = \eta(L)\exp\{2i[\delta(L) + \sigma_c(L)]\}. \qquad (1)$$

Here, $\sigma_c(L)$ is the Coulomb scattering phase, and the scattering matrix modulus $\eta(L)$ and the nuclear part of the real scattering phase $\delta(L)$ can be parametrized as follows [10, 11]

$$\eta(L) = \exp[\ln\varepsilon\ g(L, L_0, \Delta_0)], \qquad (2)$$

$$2\delta(L) = \delta_0 \; g^2(L, L_1, \Delta_1), \tag{3}$$

where $g(L, L_i, \Delta_i)$ is the Fermi step function

$$g\left(L, L_i, \Delta_i\right) = \left[1 + \exp\left(\frac{L - L_i}{\Delta_i}\right)\right]^{-1}. \tag{4}$$

Since the derivatives of step function (4), $(\Delta_i)^n d^n g(L, L_i, \Delta_i)/dL^n$, form a complete set of functions in the interval $0 \leq L < \infty$ [14] and $dg/dL = \left(g^2 - g\right)/\Delta_i$, the expressions (2) and (3) may be considered as expansions of the imaginary and real parts of the nuclear scattering phase in these functions. The fact that it is sufficient to take only the first term of such an expansion in (2) and the first two terms with equal weights in (3) follows from analyzing a lot of cross sections of scattering of different light nuclei by various target nuclei.

The quantity $\sigma_c(L)$ is taken in the form of scattering phase for the potential $V_c\left(R_c, r\right)$ of the uniformly charged sphere of radius $R_c$ (for the $^6$Li projectiles we take $R_c = 1.3A_t^{1/3}$ fm, where $A_t$ is the target mass number). The quasiclassical formula for $\sigma_c(L)$ used in the calculations is presented in [11, 13].

As the function $g(L, L_i, \Delta_i)$ in expressions (2) and (3), the symmetrized step–function can also be taken

$$g(L, L_i, \Delta_i) = \frac{\sinh\left(L_i/\Delta_i\right)}{\left[\cosh\left(L_i/\Delta_i\right) + \cosh\left(L/\Delta_i\right)\right]}. \tag{5}$$

Its advantage, as compared to the function (4), is that in this case the deflection function $\Theta(L) = (2d/dL)\left[\delta(L) + \sigma_c(L)\right]$ goes to zero at $L = 0$.

The parameters of the model have a clear physical meaning. The phase $\delta_0$ characterizes intensity of the nuclear refraction, and the parameter $\varepsilon$ determines the transparency of the nucleus in the region of small angular momenta. The quantities $L_0$ and $\Delta_0$ determine size and diffuseness of the region of strong absorption in the space of impact parameters $b = L/k$ ($k$ is the wave vector). The radius of strong absorption $R_{1/2}$ is defined as $R_{1/2} = \left(\xi + \sqrt{L_{1/2}^2 + \xi^2 - 1/4}\right)/k$, $\eta(L_{1/2}) = (1+\varepsilon)/2$, where $\xi$ is the Sommerfeld parameter. The nuclear surface diffuseness $d_0 = \Delta_0/k$ corresponds to the diffuseness of the imaginary part of optical potential as a quantity which governs the decrease rate of the imaginary part of scattering phase at large impact parameters. An analogous meaning may be given to the parameters $L_1$ and $\Delta_1$ as the quantities characterizing the region of nuclear refraction.

When analyzing the experimental data, we decompose the scattering amplitude into the near–side $f^{(-)}(\theta)$ and far–side $f^{(+)}(\theta)$ components (the N/F decomposition) corresponding to quasiclassical scattering from the near and far edges of the scatterer [2], which is very helpful for understanding the physical meaning of different interference effects in the cross sections. These components were calculated as follows:

$$f^{(\pm)}(\theta) = \mp\frac{1}{2\pi k}\sum_{l=0}^{\infty}(2l+1)[S(L) - \exp(2i\sigma_l)] \tag{6}$$

$$\times Q_l(\cos\theta \mp i\nu) + f_R^{(\pm)}(\theta) - f_{sp}^{(\pm)}(\theta), \quad \nu \to 0.$$

Here, $Q_l(x)$ are the second kind Legendre functions, $\sigma_l$ is the point–charge Coulomb scattering phase for the angular momentum $l$ and $f_R^{(\pm)}(\theta)$ are the near– and far–side components of the Rutherford amplitude $f_R(\theta)$

$$f_R^{(\pm)}(\theta) = f_R(\theta)\left\{\frac{1}{2}\left[1 \mp \frac{1 + e^{-2\pi\xi}}{1 - e^{-2\pi\xi}}\right]\right. \tag{7}$$

$$\left.\mp\frac{i}{2\pi}\left[\ln\cos^2\frac{\theta}{2} + \int\limits_{-\ln\sin^2\frac{\theta}{2}}^{\infty} dt\frac{e^{-t}\left[1 - e^{-i\xi t}\right]}{1 - e^{-t}}\right]\right\}.$$

The expressions (6) and (7) correspond to the usually employed decomposition procedure by Fuller [15], except for the terms $f_{sp}^{(\pm)}(\theta)$. This is our modification made to eliminate some physically spurious contributions into the near–side $\sigma_N(\theta) \equiv \left|f^{(-)}(\theta)\right|^2$ and far–side $\sigma_F(\theta) \equiv \left|f^{(+)}(\theta)\right|^2$ components of the cross section, whose presence is sometimes exhibited at large angles. The main part of these contributions can be removed by subtracting the spurious terms of the form [11]

$$f_{sp}^{(\pm)}(\theta) = \pm\frac{1}{2\pi k}\,\frac{S(1/2)}{1 - \cos\theta}\,. \tag{8}$$

## III. ANALYSIS OF THE EXPERIMENTAL DATA

On the basis of expressions (1)–(3), and (5) we have carried out analysis of the experimentally measured differential cross sections of the $^6$Li elastic scattering on $^{12}$C, $^{28}$Si, $^{40}$Ca, $^{58}$Ni, and $^{90}$Zr nuclei at 210 MeV and on $^{12}$C and $^{28}$Si nuclei at 318 Mev [16–18]. The results of these calculations are complemented by the results of the analysis of the experimental data [19] on $^6$Li elastic scattering by $^{12}$C, $^{40}$Ca, and $^{90}$Zr nuclei at 156 MeV, presented partially in [12]. The $S$–matrix parameters found from fitting the experimental data are presented in table 1 together with the corresponding $\chi^2$ values and the calculated values of the integrated reaction cross sections $\sigma_r$. We also present the reduced radii $r_{0,1} = L_{0,1}/\left[k\left(6^{1/3} + A_t^{1/3}\right)\right]$, $r_{1/2} = R_{1/2}/\left(6^{1/3} + A_t^{1/3}\right)$ and diffuseness values $d_0$ and $d_1 = \Delta_1/k$ in table 2. In the same place we show the nuclear rainbow angles $\theta_r$ corresponding to the minima of the found deflection functions.

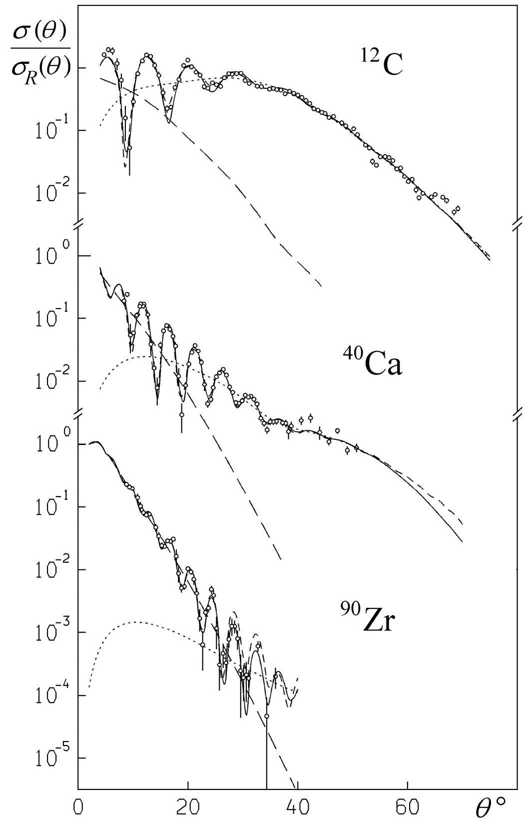


Fig. 1. The ratios of the cross sections of the 156 MeV $^6$Li elastic scattering by $^{12}$C, $^{40}$Ca, and $^{90}$Zr nuclei to the Rutherford ones. The solid lines show calculations by the $S$–matrix model, the long dashes and dots are the corresponding ratios $\sigma_N(\theta)/\sigma_R(\theta)$ and $\sigma_F(\theta)/\sigma_R(\theta)$ for the near–side and far–side cross section components. The short dashes show the optical model calculations. Experimental data are taken from [19].

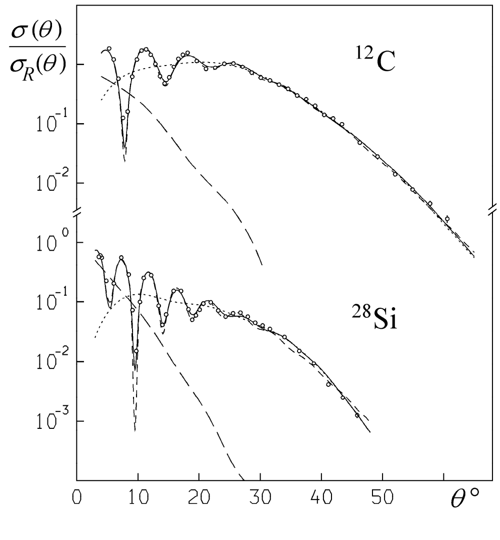


Fig. 2. The same as in fig. 1 for the scattering on $^{12}$C and $^{28}$Si nuclei at 210 MeV. Experimental data are taken from [16, 17].

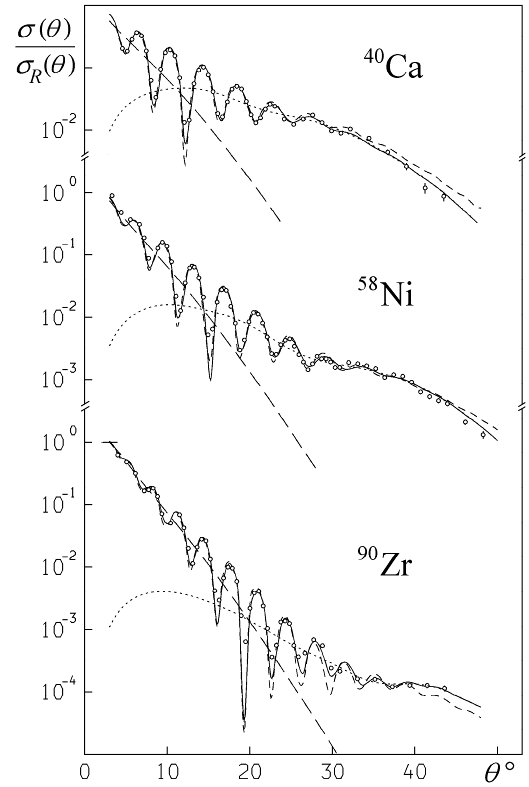


Fig. 3. The same as in fig. 1 for the scattering on $^{40}$Ca, $^{58}$Ni, and $^{90}$Zr nuclei at 210 MeV. Experimental data are taken from [16, 17].

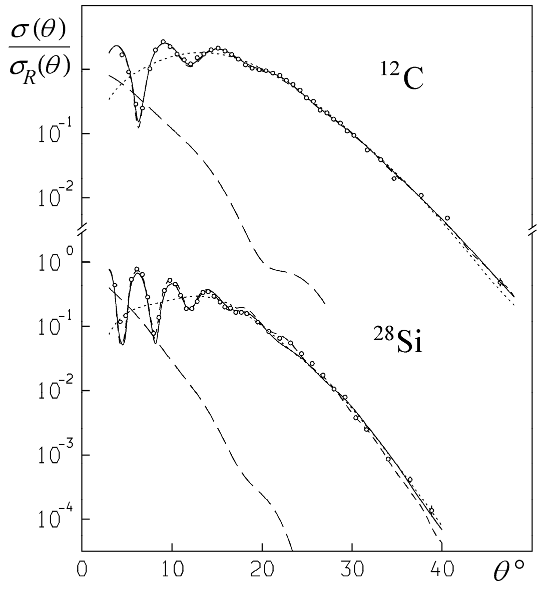


Fig. 4. The same as in fig. 1 for the scattering on $^{12}$C and $^{28}$Si nuclei at 318 MeV. Experimental data are taken from [18].

To compare with the $S$–matrix approach proposed, in all the cases under consideration calculations of the cross sections were carried out on the basis of the Woods–Saxon optical potentials found in [16–19]. The analysis carried out shows that the $S$–matrix approach allows us to obtain a good description of all considered experimental data, which does not yield to the optical model in quality (figs. 1–4). Note that the found values of the radii and diffuseness, after the main part of their dependence on the projectile energy and on the target nucleus mass number has been separated out, change rather slowly in the wide energy range and from one target nucleus to another (table 2). Here, we should mention a systematic slow decrease of the strong absorption radius $r_{1/2}$ with the energy increase. This property is also known from analyses of nuclear scattering cross sections by the optical model [20]. The transparency $\varepsilon$ grows and the parameter of nuclear refraction $\delta_0$ decreases with energy increasing and the mass number $A_t$ decreasing.

In all the cases shown in figs. 1–4, except for the scattering on $^{90}$Zr at 156 MeV, the calculated differential cross sections exhibit the nuclear rainbow effect at sufficiently large scattering angles. Three representative examples of corresponding deflection functions are shown in figs. 5 together with the $S$–matrix moduli. For the light target nuclei $^{12}$C and $^{28}$Si at all the energies, owing to relatively large transparency values, the nuclear rainbow effect is well pronounced in the form of a wide rainbow hump in the far–side component of cross section. For the heavier target nuclei $^{40}$Ca at 156 MeV and $^{40}$Ca, $^{58}$Ni, and $^{90}$Zr at 210 MeV the transparency is much smaller, which results in the fact that the nuclear rainbow is manifested not so distinctly—as a shoulder in the far–side component at large scattering angles. The presence of this shoulder is clearly disclosed by the N/F decomposition of the cross section, whereas in the summarized cross section it is rather disguised by diffraction oscillations. Such a weak manifestation of the nuclear rainbow effect is usually called the rainbow “ghost” [2].

In the case of the $^{90}$Zr target at 156 MeV, the transparency value is too small and the rainbow angle is too large for observing nuclear rainbow in the angular range studied. The existence of the rainbow ghosts for $^{40}$Ca at 156 MeV and $^{90}$Zr at 210 MeV cannot also be considered as firmly established because of the lack of experimental points at sufficiently large scattering angles. For these three cases, this circumstance caused a discrete ambiguity of the optical potentials in [17, 19] and also makes determination of the $S$–matrix parameters less unambiguos, than for the light target nuclei $^{12}$C and $^{28}$Si and for $^{40}$Ca and $^{58}$Ni at 210 MeV. The near–side cross section components in figs. 1–4 show a regular quick exponential decrease characteristic of a Fraunhofer–type amplitude. As a result, a quick Fraunhofer crossover occurs in all the cross sections, which causes the quickly damped Fraunhofer oscillations at small angles and the

| Nucleus | E, MeV | $L_0$ | $L_1$ | $\Delta_0$ | $\Delta_1$ | $\varepsilon$ | $\delta_0$ | $\sigma_r$, mb | $\chi^2$ |
|---|---|---|---|---|---|---|---|---|---|
| $^{12}$C | 156 | 18.68 | 15.50 | 3.50 | 5.29 | $3.16\cdot10^{-2}$ | 16.10 | 1175 | 8.0 |
| $^{40}$Ca | 156 | 30.69 | 24.48 | 5.07 | 8.45 | $1.71\cdot10^{-3}$ | 34.90 | 1997 | 9.9 |
| $^{90}$Zr | 156 | 39.27 | 30.82 | 5.91 | 9.06 | $1.70\cdot10^{-4}$ | 59.38 | 2809 | 1.3 |
| $^{12}$C | 210 | 20.02 | 14.38 | 4.39 | 7.65 | $4.17\cdot10^{-2}$ | 23.16 | 1088 | 9.7 |
| $^{28}$Si | 210 | 33.07 | 24.49 | 5.24 | 10.10 | $2.76\cdot10^{-2}$ | 25.03 | 1623 | 10.2 |
| $^{40}$Ca | 210 | 36.38 | 29.81 | 5.82 | 9.82 | $6.60\cdot10^{-3}$ | 27.37 | 1922 | 13.3 |
| $^{58}$Ni | 210 | 39.51 | 31.83 | 6.03 | 10.52 | $3.00\cdot10^{-3}$ | 33.26 | 2090 | 9.8 |
| $^{90}$Zr | 210 | 46.53 | 35.65 | 6.47 | 11.31 | $6.20\cdot10^{-4}$ | 53.81 | 2679 | 11.0 |
| $^{12}$C | 318 | 23.68 | 16.49 | 6.01 | 10.21 | $5.64\cdot10^{-2}$ | 22.24 | 1080 | 2.9 |
| $^{28}$Si | 318 | 38.70 | 30.14 | 6.72 | 12.36 | $4.56\cdot10^{-2}$ | 19.89 | 1479 | 5.3 |

Table 1. The $S$–matrix parameters for the $^6$Li elastic scattering by nuclei.

| Nucleus | E, MeV | $r_0$, fm | $r_1$, fm | $r_{1/2}$, fm | $d_0$, fm | $d_1$, fm | $\theta_r^\circ$ | $\theta^\circ_{r,\text{ op}}$ |
|---|---|---|---|---|---|---|---|---|
| $^{12}$C | 156 | 1.019 | 0.845 | 1.324 | 0.784 | 1.185 | 44.8 | 55.5 |
| $^{40}$Ca | 156 | 1.003 | 0.800 | 1.413 | 0.868 | 1.446 | 58.8 | 83.1 |
| $^{90}$Zr | 156 | 0.988 | 0.775 | 1.447 | 0.934 | 1.435 | 97.1 | 108.9 |
| $^{12}$C | 210 | 0.941 | 0.675 | 1.243 | 0.847 | 1.477 | 37.0 | 40.7 |
| $^{28}$Si | 210 | 1.061 | 0.786 | 1.347 | 0.816 | 1.573 | 33.2 | 42.3 |
| $^{40}$Ca | 210 | 1.023 | 0.838 | 1.371 | 0.857 | 1.446 | 39.4 | 49.0 |
| $^{58}$Ni | 210 | 0.980 | 0.790 | 1.339 | 0.851 | 1.484 | 44.5 | 55.9 |
| $^{90}$Zr | 210 | 1.007 | 0.771 | 1.397 | 0.881 | 1.541 | 69.9 | 65.1 |
| $^{12}$C | 318 | 0.904 | 0.629 | 1.207 | 0.942 | 1.601 | 23.3 | 23.5 |
| $^{28}$Si | 318 | 1.007 | 0.784 | 1.263 | 0.848 | 1.561 | 21.6 | 24.1 |

Table 2. The reduced radii, diffuseness values and rainbow angles ($\theta_{r,\text{ op}}$ are the optical–model values) for the $^6$Li elastic scattering by nuclei.

complete dominance of the far–side component in the region of large scattering angles.

The comparison of the results obtained on the basis of the $S$–matrix approach with the corresponding calculations by the optical model shows certain similarity in some aspects. Both models yield fitting of the experimental data which is of equal value and quality, although sometimes some distinctions between the calculated cross sections are observed in the region of quick decrease of the rainbow cross section (on the dark side of the rainbow). The integrated reaction cross sections calculated by the optical model practically coincide with those presented in table 1. The most significant distinction for $^{90}$Zr at 210 MeV ($\sigma_{r,\,\mathrm{op}} = 2613$ mb) is of 2.5%. The values of the strong absorption radius $R_{1/2}$ are also practically the same in both models. Figs. 5 show that the scattering matrices calculated in both models are very close to each other in the peripheral region of impact parameters. The $S$–matrix moduli coincide at $b > R_{1/2}$, and the real scattering phases, in most cases, are close even at values of $b$ somewhat smaller than the mentioned above.

Thus, the character of nuclear absorption and refraction of scattered waves at the nuclear boundary is similar for both models.

The qualitative behavior of the functions $\eta(L)$ and $\Theta(L)$ is similar in the $S$–matrix approach and in the optical model for $^{12}$C and $^{28}$Si nuclei at all the energy values and for $^{40}$Ca and $^{58}$Ni at 210 MeV (see fig. 5, b, c). This similarity is due to the fact that in these cases the projectile energy is sufficiently higher, than the critical one, $E_{\mathrm{cr}}$, below which the nuclear rainbow effect disappears [4]. In terms of the potential approach, $E_{\mathrm{cr}}$ corresponds to the maximum height of the outer centrifugal barrier at the $L$ value large enough in order that a pocket in the real effective potential became filled in [4]. In other words, $E_{\mathrm{cr}}$ is the energy value below which an orbiting phenomenon would exist in classical scattering. The $E_{\mathrm{cr}}$ value increases with the target mass number increase [4]. The most pronounced qualitative distinction of the optical–model $\eta(L)$ and $\Theta(L)$ from ours occurs for $^{90}$Zr at 156 MeV (fig. 5, a). The dip in the $S$–matrix modulus and the complicated behavior of the deflection function near the surface region, observed for the optical–model calculation, can be explained by the existence of a Regge pole here, lying not very far from the real $L$ axis. Such poles can play a significant role in the energy region below $E_{\mathrm{cr}}$ (the resonant region) [21]. In terms of the semiclassical approach these effects are ascribed to interference between the wave reflected from the outer barrier and the one that penetrates through the barrier and is reflected from the inner wall of the potential pocket [22]. The $S$–matrix model in the form used does not take account of such Regge poles whose effect, however, could be manifested at much larger scattering angles. A generalization of the model for this case is proposed in [23].

Even in the cases when both models yield a similar qualitative behavior of $\eta(L)$ and $\Theta(L)$, there are significant distinctions between them. In the optical model, the $S$–matrix modulus at $b < R_{1/2}$ changes steeper. In all

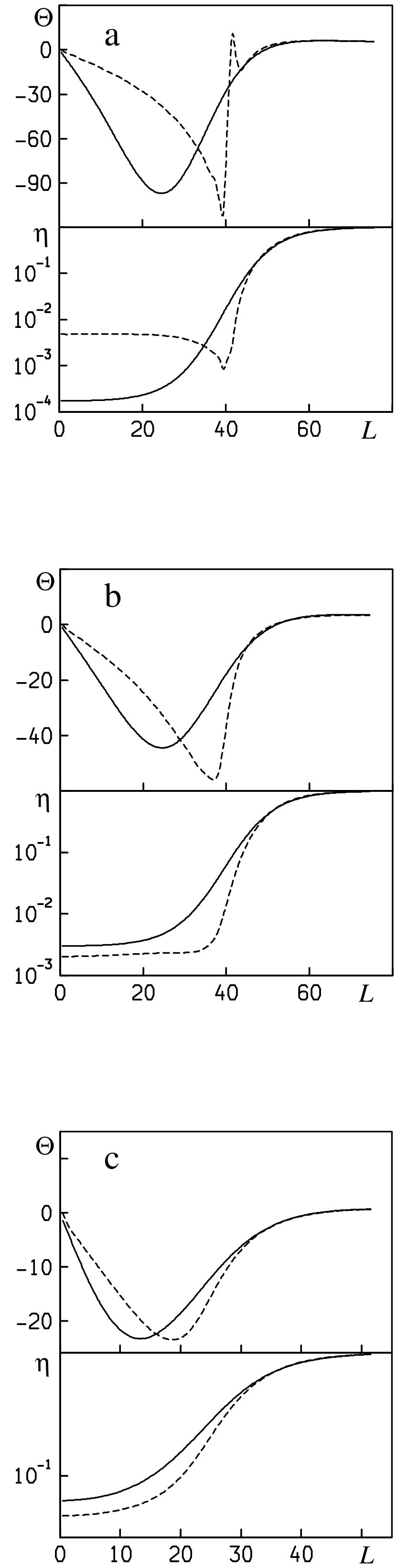


Fig. 5. Deflection functions $\Theta(L)$ (degrees) and $S$–matrix moduli $\eta(L)$ for the $^{6}$Li elastic scattering by $^{90}$Zr nuclei at 156 MeV (a), by $^{58}$Ni nuclei at 210 MeV (b), by $^{12}$C nuclei at 318 MeV (c). The solid lines show calculations by the $S$–matrix model, the dashes show the optical–model calculations.

the cases, the deflection function minimum, corresponding to the rainbow point, lies closer to the surface region. This distinction is essential, because the occurrence of the rainbow point in the $S$–matrix approach at small impact parameters might mean that the corresponding angular distributions allow one to probe a deeper nuclear domain. There are also distinctions in the found rainbow angles (table 2). However, when the rainbow angles and sharpness of the rainbow minima differ significantly (see fig. 5, b), the decrease rate of the cross sections on the dark side of the rainbow are different, too. This distinction of the cross sections is not large, but it promises to become highly considerable at large $\theta$ where experimental data are absent. At the same time, in the case of scattering on $^{12}$C nuclei at $E = 318$ MeV, for which the found rainbow angles coincide and the character of the rainbow minima is similar (fig. 5, c), the cross sections calculated in both models are almost identical in the angular range under consideration. Thus, we may conclude that analysis of the experimental data in the considered angular range still leaves room for determining both the $S$–matrix parameters and the optical potentials more precisely, although it has removed the discrete ambiguity of the potentials in some cases [16–19].

The calculations carried out show that the proposed $S$–matrix approach makes it possible to describe the experimentally measured cross sections of the $^6$Li elastic scattering by different target nuclei in a wide energy range not worse, than the optical model does, and reproduces successfully the physically different diffraction and refraction effects observed. Along with a certain similarity of the results obtained in this approach and by the optical model, there also exist considerable distinctions between them. To elucidate the relation between these two models, an analysis of experimental data in a wide range of scattering angles is necessary.

## ACKNOWLEDGMENTS

I am indebted to A. Nadasen for sending me tables of the experimental data and to Yu. A. Berezhnoy for a valuable discussion of this work. This work was supported, in part, by the State Foundation for Fundamental Research of Ukraine, grant No. 2.4/416.

[1] W. E. Frahn, *Diffractive Processes in Nuclear Physics* (Clarendon Press, Oxford, 1985).
[2] M. S. Hussein, K. W. McVoy, Prog. Part. Nucl. Phys. **12**, 103 (1984).
[3] G. R. Satchler, *Direct nuclear reactions* (Clarendon Press, Oxford, 1983).
[4] D. A. Goldberg, S. M. Smith, Phys. Rev. C **7**, 1938 (1973).
[5] W. E. Frahn, R. H. Venter, Ann. Phys. **24**, 243 (1963).
[6] T. E. O. Ericson, in *Preludes in Theoretical Physics*, edited by A. de-Shalit, H. Feshbach, L. van Hove (North–Holland, Amsterdam, 1965), p. 321.
[7] J. A. McIntyre, K. H. Wang, L. C. Becker, Phys. Rev. **117**, 1337 (1960).
[8] Yu. A. Berezhnoy, A. V. Kuznichenko, G. M. Onishchenko, V. V. Pilipenko, Sov. J. Part. Nucl. **18**, 121 (1987).
[9] M. C. Mermaz, Z. Phys. A **321**, 613 (1985).
[10] V. V. Pilipenko, Dopovidi AN URSR A, No. 1, 65 (1989).
[11] Yu. A. Berezhnoy, V. V. Pilipenko, Mod. Phys. Lett. A **10**, 2305 (1995).
[12] Yu. A. Berezhnoy, V. V. Pilipenko, Izv. RAN., Ser. fiz. **59**, 197 (1995).
[13] Yu. A. Berezhnoy, V. V. Pilipenko, Heavy Ion Phys. **3**, 249 (1996).
[14] B. I. Tishchenko, E. V. Inopin, Sov. J. Nucl. Phys. **7**, 618 (1968).
[15] R. C. Fuller, Phys. Rev. C **12**, 1561 (1975).
[16] A. Nadasen, M. McMaster, G. Gunderson *et al.*, Phys. Rev. C **37**, 132 (1988).
[17] A. Nadasen, M. McMaster, M. Fingal *et al.*, Phys. Rev. C **39**, 536 (1989).
[18] A. Nadasen, T. Steven, J. Farnat *et al.*, Phys. Rev. C **47**, 674 (1993).
[19] J. Cook, H. J. Gils, H. Rebel, Z. Majka, H. Klewe–Nebenius, Nucl. Phys. A **388**, 173 (1982).
[20] N. Alamanos, F. Auger, J. Barrette *et al.*, Phys. Lett. B **137**, 37 (1984).
[21] K. W. McVoy, Phys. Rev. C **3**, 1104 (1971).
[22] D. M. Brink, N. Takigawa, Nucl. Phys. A **279**, 159 (1977).
[23] V. V. Pilipenko, Mod. Phys. Lett. A **13**, 211 (1998).

## ФЕНОМЕНОЛОГІЧНИЙ $S$–МАТРИЧНИЙ ПІДХІД ДО ВИВЧЕННЯ ПРУЖНЬОГО РОЗСІЯННЯ ЯДЕР $^6$Li АТОМНИМИ ЯДРАМИ

В. В. Пилипенко
*Харківський державний університет,*
*майдан Свободи, 4, Харків, 310077, Україна*

Недавно запропоновану оригінальну $S$–матричну модель застосовано для аналізу диференціяльних перерізів пружнього розсіяння ядер $^6$Li різними ядрами мішені при різних значеннях енергії. Результати цього аналізу порівнюємо з аналогічними результатами, отриманими за допомогою оптичної моделі.